

Exponential behavior of the Ohmic transport in organic films

Corneliu N. Colesniuc,^{1,*} Rudro R. Biswas,² Samuel A. Hevia,^{1,3} Alexander V. Balatsky,⁴ and Ivan K. Schuller¹¹*Department of Physics and Center for Advanced Nanotechnology, University of California San Diego, La Jolla, California 92093, USA*²*Department of Physics, Harvard University, Cambridge, Massachusetts 02138, USA*³*Facultad de Física, Universidad Católica de Chile, Casilla 306, Santiago, Chile 6904411*⁴*Theoretical Division and Center for Integrated Nano-Technologies, Los Alamos National Laboratory, Los Alamos, New Mexico 87545, USA*

(Received 3 October 2010; published 18 February 2011)

An exponential dependence of conductance on thickness and temperature was found in the low-voltage, Ohmic regime of copper (CuPc) and cobalt (CoPc) phthalocyanine, sandwiched between palladium and gold electrodes unlike ever claimed in organic materials. To assure cleanliness and integrity of the electrode-phthalocyanine interface, the devices were prepared *in situ*, using organic molecular beam deposition with a floating shadow mask. The dc transport measurements in a wide temperature and thickness range show that (i) the low-voltage J - V curve is linear, with current increasing sharply at higher voltages, (ii) the low-voltage conductance increases exponentially with temperature, and (iii) it decreases exponentially with film thickness. A comparison with conventional models fails to explain all the data with a single set of parameters. On the other hand, a model outlined here, which incorporates tunneling between localized states with thermally induced overlap, agrees with the data and decouples the contributions to conductance from the electrode-film interface and the bulk of the film.

DOI: [10.1103/PhysRevB.83.085414](https://doi.org/10.1103/PhysRevB.83.085414)

PACS number(s): 73.40.Sx, 73.50.Dn, 73.61.Ph

I. INTRODUCTION

Metallophthalocyanines (MPc) have been studied for many decades and many of their properties are well understood.¹ They serve as a model system for the whole class of flat, organic molecules, are usually p -type semiconductors, and have been the subject of much research due to their unique structural, electrical, and optical properties.² An important challenge in the study of electrical transport in organic molecules is to identify the charge transport mechanisms that determine the temperature and size (length or thickness) dependence of the current-voltage (J - V) characteristics. A linear J - V characteristic at low voltages followed by nonlinear V dependences at higher voltages was claimed in many cases.³⁻⁷ Generally, the current density in the linear (“Ohmic”) regime was expected to be given as $J = n\mu qV/L$, although an explicit length or thickness dependence experimental study is usually lacking. Many other studies investigate only the high-voltage dependence, overlooking altogether the low-voltage regime.⁸⁻¹² The temperature dependence of the current in the Ohmic regime is usually characterized using Arrhenius plots, in which the slopes of the linear regions give the activation energies for hopping transport.^{5,7,13} All these studies are generally characterized by a lack of comprehensive experimental investigations in a wide parameter range, and a complete theory that can simultaneously and correctly describe the voltage, thickness, and temperature dependence of the current.

In strong contrast, we performed a detailed study of the low-voltage J - V characteristics in CuPc and CoPc thin films. Interestingly, over broad thickness and temperature ranges, the Ohmic conductance decreases exponentially with the organic layer thickness, and increases exponentially with temperature. This behavior can be described with a single model in which thermal molecular fluctuations change the local energies and the overlap between localized-states wave functions, such that the carriers can tunnel between these states.

II. EXPERIMENT

CuPc and CoPc powder, purified by gradient sublimation, was used to prepare sandwich devices between palladium and gold electrodes in an organic molecular beam deposition (OMBD) system with a base pressure of 10^{-10} torr, on c -plane sapphire substrates. Using a floating shadow mask positioned $50\ \mu\text{m}$ from the substrate, six pairs of bottom electrodes were first deposited, covered by different thickness CuPc or CoPc layers, and then a top common electrode completed the devices. The lateral size of the devices was $127\ \mu\text{m}$. The *in situ* capability allows the growth of devices with clean interfaces. The deposition rates for the bottom electrodes and the organic layers were 0.2 and $0.3\ \text{\AA}/\text{sec}$ respectively, while for the top electrode, the deposition rate was $10\ \text{\AA}/\text{sec}$. A large deposition rate for the top electrode suppresses the diffusion of metal atoms into the organic layer by favoring the formation of larger, less mobile metal clusters.¹⁴

The MPc thin-film structure is controlled by several factors, including the substrate type and temperature.² The interplay between the intermolecular and the molecule-substrate interactions determines the molecular growth. If the intermolecular interactions are stronger than the molecule-substrate interaction, the molecules grow vertically, whereas in the opposite case (as for metallic substrates), they grow parallel to the substrate.^{2,15}

To check the effect of the electrodes, several samples with palladium and gold electrodes were fabricated. To eliminate as much as possible any systematic errors, several “devices” were fabricated under identical evaporation conditions on each substrate (“sample”). More than 40 samples were fabricated and measured. Devices made with palladium (Pd/MPc/Pd) and gold (Au/MPc/Au) electrodes, and using both CuPc and CoPc, have the same thickness and temperature behavior of the conductance. Devices with palladium electrodes are more stable, have less noise, and a longer lifetime compared to devices with gold electrodes. This may be due to different

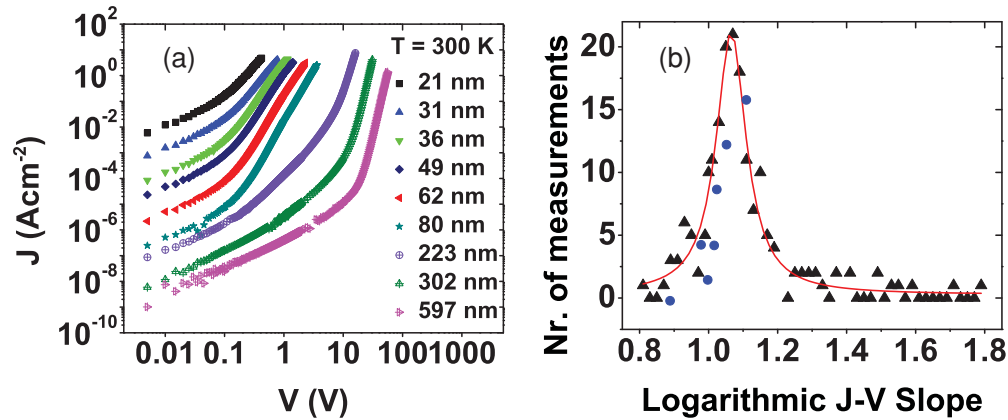


FIG. 1. (Color online) (a) Logarithmic plots of current density as a function of applied voltage at 300 K for Pd/CuPc/Pd devices with different organic layer thickness. Positive bias was applied on the bottom electrode. (b) Distribution of the low-voltage logarithmic J - V slopes for all measurements. The continuous line is a Lorentzian fit of the data. The blue circles include the slope values corresponding to the data shown in (a).

growth mechanisms of the two metals, with palladium favoring the coalescence of a continuous film at small thicknesses,¹⁴ and gold having a higher tendency to diffuse into the organic layer.¹⁶

The dc current-voltage curves were measured in the dark and in a vacuum at 10^{-4} torr using an electrometer. The resistance of the devices is several orders of magnitude larger than the total resistance of the wires and electrodes; therefore, the errors introduced by the two-probe measurement are negligible.

III. EXPERIMENTAL RESULTS

Current-voltage characteristics were measured on devices with the organic layer thickness ranging from 21 to 597 nm. Figure 1(a) shows, for clarity, a representative set of 300 K data on a logarithmic scale for Pd/CuPc/Pd devices from three different samples. The J - V curves exhibit two distinct regions: linear at low voltage, followed by a nonlinear region at higher voltages. At low voltages, the transport is Ohmic, as determined from the logarithmic slopes of the J - V curves.

Figure 1(b) shows the distribution of the logarithmic slopes for all measurements. The Lorentzian fit of the data is centered at 1.06, has a 0.1 width at half-maximum, and is slightly asymmetrical toward values larger than 1. Possibly, the slight asymmetry is due to the finite contribution from charge carriers injected from the electrodes, favoring a higher-order term in the conductance at higher voltages. Nevertheless, Fig. 1(b) shows that most slopes are closely distributed around 1, proving the Ohmic behavior in the low-voltage regime.

In order to investigate the transport mechanism, the thickness and temperature dependence of the current was measured. The conductance per unit area, G/A is shown in Fig. 2(a) as a function of the thickness at 300 K. The conductance decreases exponentially by 5 orders of magnitude from 21 to 80 nm, while above 100 nm, the drop rate is much smaller. To investigate any uncontrolled effects related to sample fabrication, we prepared a fourth sample with devices ranging in thickness between 60 and 400 nm, shown as red circles in Fig. 2(a). Although the values of the conductance for a fixed thickness may differ by as much as an order of magnitude from sample to sample, the behavior is similar: at

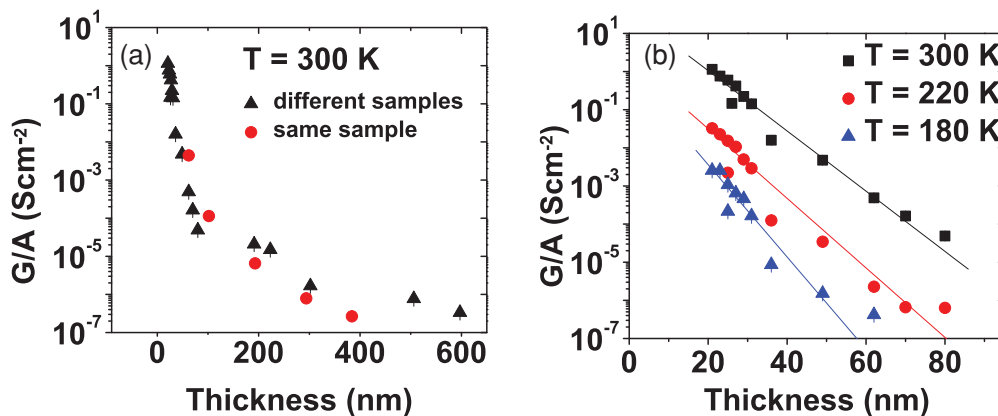


FIG. 2. (Color online) (a) Conductance per unit area as function of the organic layer thickness for Pd/CuPc/Pd devices. Black triangles: devices grown on different samples; the decrease is very sharp for thicknesses up to 100 nm, but becomes much slower for thicknesses larger than 100 nm. Red circles: devices grown on the same sample show a similar behavior. (b) Thickness dependence of conductance at different temperatures. The straight lines are fits to the data. The drop in conductance becomes steeper at lower temperatures.

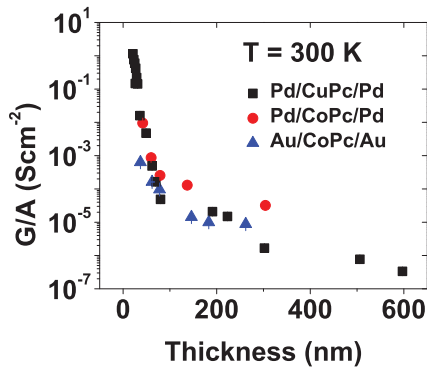


FIG. 3. (Color online) Thickness dependence of conductance per unit area for devices with palladium and gold electrodes and CuPc and CoPc as the organic layer. The behavior is similar for all samples: The decrease is very sharp for thicknesses up to 100 nm, but becomes much slower for thicknesses larger than 100 nm.

small thicknesses, the rate of decrease is much larger than above 100 nm. Furthermore, below 100 nm, the thickness dependence changes with the temperature. As Fig. 2(b) shows, the exponential drop of the conductance becomes steeper at lower temperatures. A similar thickness dependence is observed in Pd/CoPc/Pd and Au/CoPc/Au devices, as shown in Fig. 3. The conductance drops exponentially below 100 nm, while above 100 nm, the decrease is much slower.

Figure 4 is a plot of the conductance per unit area as a function of temperature for selected, representative devices (for clarity), spanning the entire thickness range together with fits to commonly accepted models. In Fig. 4(a), the data are plotted assuming a nearest-neighbor hopping model with an activated conductivity.¹⁷ It is clear that a single activation energy can not be obtained for the whole temperature range. In Fig. 4(b), the data are plotted according to the variable-range hopping model.¹⁸ Again, the data can not be fitted with a single straight line across the whole temperature range. Therefore, both fits imply the existence of multiple transport regimes as a function of temperature within these models. Perhaps, the failure of the fit to these models is indicative of another possible mechanism being operational.

On the other hand, the semilogarithmic plot in Fig. 4(c) shows that the experimentally measured temperature dependence of the conductance can be described with a single exponential dependence for all devices in the whole temperature range. For thicker films, the low-voltage region can not be resolved at lower temperatures and, therefore, the number of data points decreases with increasing thickness. In the thinnest devices, the conductance increases by 6 orders of magnitude from 20 K to 320 K. This exponential dependence spans the entire temperature range, regardless of the organic layer thickness, and suggests a universal behavior for all devices.

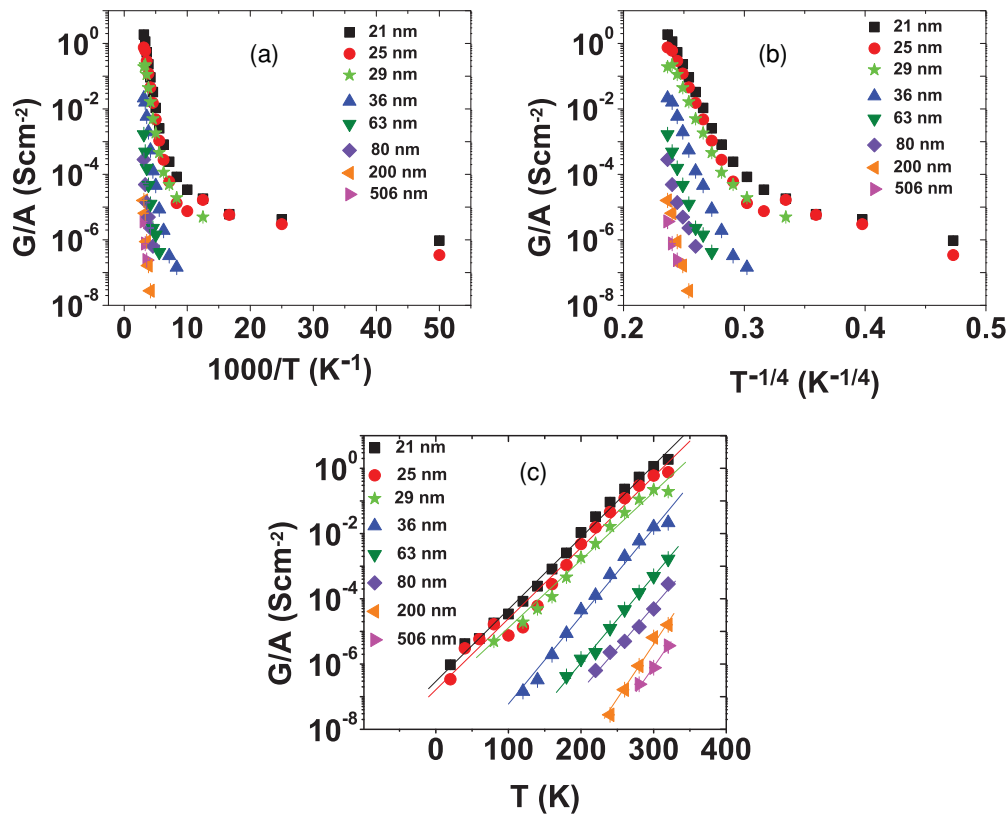


FIG. 4. (Color online) (a) Plot of conductance per unit area vs temperature for selected data sets for a nearest-neighbor hopping model with an activated conductivity. No single activation energy can be obtained for the whole temperature range. (b) Plot of the same data assuming a variable-range hopping model. Data can not be fitted with a single straight line across the whole temperature range. (c) Semilogarithmic plot of conductance per unit area vs temperature. All devices show a similar exponential dependence, suggesting a universal behavior for the whole temperature range.

The experimental results found here are characterized by an Ohmic low-voltage regime, which depends exponentially on thickness and temperature. Note that this behavior is characteristic for wide thickness (20–100 nm) and temperature (20–320 K) ranges, and is present in samples made with palladium and gold electrodes for both CuPc and CoPc. Therefore, it is reasonable to inquire whether a single theoretical model can simultaneously explain all the properties mentioned above. While some of these have been encountered occasionally in some systems, none have been claimed together or in a broad experimental parameter range.

The experimental results presented here are based on experimental work over more than a two-year period, and the consistency of the results over many samples and different sample preparations imply that there are no substantial random errors present. To avoid systematic errors, randomized sample preparations and changes in the range of device parameters on a single sample were also investigated, all giving consistent results.

IV. THEORY AND DISCUSSION

Exponential thickness dependences of the conductance have been claimed before in a variety of circumstances and materials systems. An exponential dependence of the current on the organic layer thickness was observed in self-assembled monolayers between metallic electrodes.^{19,20} The thickness of those devices is of the order of 10 Å; therefore, a coherent tunneling model may apply.²¹ The devices studied here have thicknesses of at least 210 Å, so a coherent tunneling model is very improbable. An exponential increase of conductance with temperature was found in colloidal CdSe nanorods²² in the high-voltage regime, due to Fowler-Nordheim tunneling with a temperature-dependent energy gap. However, this gives a quadratic²³ (i.e., non-Ohmic) voltage dependence and, therefore, does not apply here either. The exponential temperature dependence observed in monolayers of eicosanoic acid (C₂₀) sandwiched between platinum electrodes²⁴ was explained using two models. The first model was thermionic field emission through a triangular barrier, while the second was tunneling through a thermally fluctuating barrier. The thermionic field emission is not applicable here because it gives an exponential dependence of the current on voltage.²⁵ The second model implies that thermal fluctuations produce fluctuations in the barrier width or height.

A universal, exponential temperature dependence of conductivity was found by Hurd²⁶ in low-conductivity semiconductors. He derived a tunneling model in which the barrier width vibrates as a result of thermally induced fluctuations in the overlap of the localized-states wave functions. This model was used to fit conductivity data for 10 different inorganic semiconductors: In-doped CdS, Cr-doped GaAs, As₂Te₃, Ti-doped VO₂, TaS₂, Ti₇O₁₃, SiO₂, Fe₃O₄, V₅O₉, and nAs₃₀Te₄₈Si₁₂Ge₁₀. The model could fit the data up to 7 orders of magnitude in conductivity and a factor of 4 in temperature.

Here we propose a model in which the concept of tunneling between localized states with thermally induced overlap²⁶ is used to explain the same behavior for the case of organic semiconductors. We generalize Hurd's model by deriving an expression for the conductance of the sample, which

includes both the temperature and thickness dependence. In the following, we address this model as thermally assisted sequential tunneling (TAST).

The model considers sites $i = 1, 2, \dots, N$, where electrons can occupy levels with energies E_i . According to the conventional approach, the electron can hop to a site E_j that is close enough for the overlap of wave functions to be significant, while the difference $|E_j - E_i|$ is small. This picture of tunneling in the rigid environment allows only the thermal fluctuations of the bath to broaden the energy of electrons. In organic materials and at higher temperature, the situation is different: the molecular fluctuations are significant, and they change the overlaps and local energies. In this fluctuating environment, the energy of the electron on site E_i is time dependent. For any given pair of sites E_i and E_j , the energy difference will depend on the molecular configurations, such that for some of those configurations the energies will become close. Moreover, the fluctuations produce a time-dependent alignment of groups of molecules between the two sites, such that, at a particular time, a favorable path forms and the carrier can tunnel between them. We expect that substantial fluctuations will allow relatively large sets of molecules to form an assisted tunneling path that is quite long (typically, we assume the number of molecules in the path to be greater than, or on the order of, 10 molecules). This is different from direct tunneling in which the tunneling length is on the order of 1 Å, considering that the highest occupied molecular orbital-lowest unoccupied molecular orbital (HOMO-LUMO) gap in these molecules is 1.7 eV.²⁷ The assisted tunneling considered here, while longer in range, remains incoherent in the sense that the electron does not propagate ballistically along the molecular backbone, and its phase is lost after each jump.

To make the TAST model specific, Fig. 5(a) shows a schematic of the molecular stacks grown on a palladium electrode as found by our structural studies. We assume that the carriers propagate between stacks and between molecules as shown by arrows, jumping from one molecule to another.

The conductance is therefore proportional to the total transmission probability through the stack, which is, in turn, given by the product of the transmission probabilities between individual molecules. We assume that the transmission probability from site i to site j is given by a step barrier $t_{ij} \approx e^{-\Phi_{ij}}$, where $\Phi_{ij} \propto a_{ij}\sqrt{mU_{ij}}/\hbar$ and a_{ij} and U_{ij} are the barrier width and height, respectively, for tunneling between sites i and j . Similarly, we assume that the transmission probabilities from the molecules to the up/down electrodes are those through the corresponding potential barriers $t_{U/D} \approx e^{-\Phi_{U/D}}$. The total conductance is thus proportional to the total transmission probability $G \propto e^{-(\Phi_U + \Phi_D)} \prod_{ij} e^{-\Phi_{ij}}$, with sites i and j belonging to the assisted path. The Φ_{ij} is assumed linearly dependent on a fluctuating Gaussian parameter y_{ij} (e.g., the width of the barrier), linearly related to the distance between the sites, which might, for instance, be fluctuating due to a vibrational mode

$$\Phi_{ij} \approx \Phi_0 + \alpha y_{ij}, \quad P(y) \propto e^{-y^2/T}. \quad (1)$$

Even though only large fluctuations are responsible for the formation of long-range tunneling paths, in the following, we model the fluctuations as Gaussian. This is a simplifying assumption that allows an analytical calculation of the

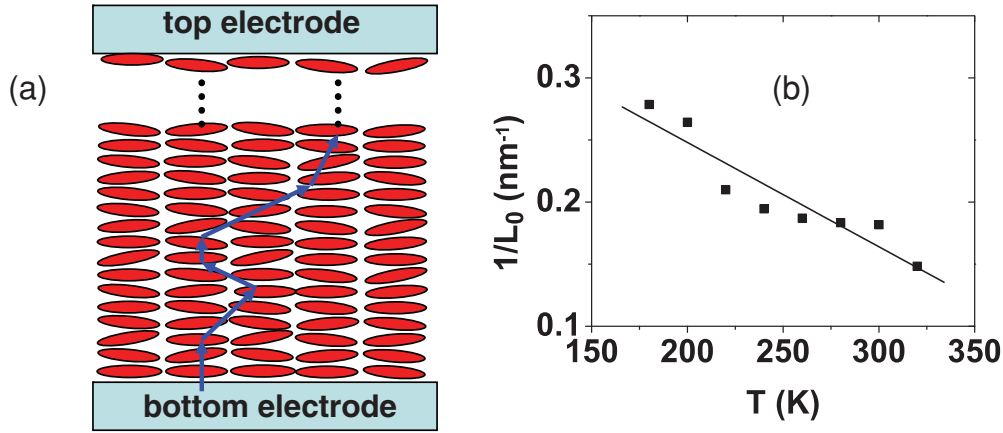


FIG. 5. (Color online) (a) Molecular stacks grown on a palladium electrode. The carriers hop from one molecule to another whenever a favorable path forms. (b) Slopes of the linear fits from Fig. 2(b) as function of temperature. The straight line is a fit of the data. The slope decreases when the temperature increases in agreement with Eq. (4).

conductance. A more realistic analysis, which includes only large fluctuations, would need to be developed. Similarly, for the molecule-electrode barriers (up and down), it is assumed that

$$\Phi_{U/D} \approx \Phi_0^{U/D} + \alpha_{U/D} y_{U/D}, \quad P(y_{U/D}) \propto e^{-y_{U/D}^2/T}. \quad (2)$$

With this, the thermally averaged stack conductance becomes

$$\begin{aligned} \langle G \rangle &\propto e^{-N\Phi_0} \prod_{\text{path}} \int_{-\infty}^{\infty} e^{-\alpha y_{ij}} e^{-y_{ij}^2/T} dy_{ij} \prod_{j=U,D} \\ &\times \int_{-\infty}^{\infty} e^{-\alpha_j y_j} e^{-y_j^2/T} dy_j \propto e^{-N\Phi_0} e^{N\alpha^2 T/4} e^{(\alpha_U^2 + \alpha_D^2)T/4} \\ &\approx e^{-L(\Phi_0/l - \alpha^2 T/4l)} e^{(\alpha_U^2 + \alpha_D^2)T/4} = e^{-L/L_0(T)} e^{(\alpha_U^2 + \alpha_D^2)T/4}, \end{aligned} \quad (3)$$

with $N \approx L/l$ the number of sites in the path, l the thermally averaged distance between two adjacent sites, L the height (thickness) of the entire stack, and

$$\frac{1}{L_0(T)} = \frac{\Phi_0}{l} - \frac{\alpha^2 T}{4l} \equiv A - BT \quad (4)$$

a linearly decreasing function of temperature. This is in agreement with the data [Fig. 5(b)] obtained from the slopes of the linear fits in Fig. 2(b).

In Eq. (3), we assume that the product over different paths will self-average to produce the number of terms that scales with the thickness of the organic layer, as excessive meandering would be less likely. The conductance can be written as $\langle G \rangle \propto e^{-AL + (BL + C)T}$, where $C = (\alpha_U^2 + \alpha_D^2)/4$. Figure 6 shows a fit of the data with this functional dependence for the Pd/CuPc/Pd devices. The plots for each thickness

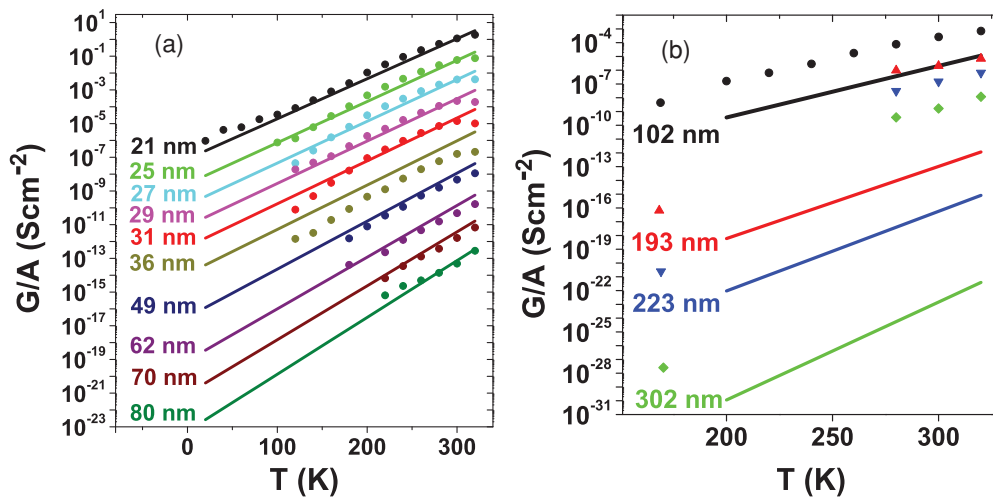


FIG. 6. (Color online) (a) Fit of the data for the Pd/CuPc/Pd devices using the functional dependence derived in Eq. (3). The model (solid lines) can fit the experimental values of the conductance (dots) for all temperatures, and for thicknesses up to 100 nm. Data and corresponding fit for each thickness have been shifted along the y axis for clarity; the data and fit values corresponding to the 21 nm device were not changed; all the other data sets and fit values, starting with the 25 nm device, were multiplied in consecutive order by 0.1, 0.01, and so on. (b) Above 100 nm, the model no longer fits the data. Data and corresponding fit values for the 102 nm device were not changed, while for the thicker devices, they were shifted along the y axis as described in (a).

have been shifted along the y axis for clarity. The data and the corresponding fit values for the 21 nm device [Fig. 6(a)] and the 102 nm device [Fig. 6(b)] were not changed, while the rest of the data and fit values were multiplied in consecutive order by 0.1, 0.01, and so on, starting with the 25 nm device in Fig. 6(a) and with the 193 nm device in Fig. 6(b). This model fits the experimental data for all temperatures and for thicknesses up to 100 nm. Above 100 nm, the thickness dependence is no longer exponential, which implies that some other mechanism becomes important. The temperature dependence is controlled by two parameters, B and C . From the fit, we obtain $B = 0.00045 \text{ nm}^{-1} \text{ K}^{-1}$ and $C = 0.046 \text{ K}^{-1}$. The B parameter is multiplied by the film thickness in the exponent, so our model implies that, for thinner films (thickness below 50 nm), the temperature dependence is controlled mainly by the interface, while for thicker films (thickness around 100 nm), both the interface and the film contribute equally to the exponential temperature dependence.

An interesting feature unexplained within this model is the slope change of the thickness dependence in Fig. 2(a). This may be a consequence of experimental issues, such as the thickness dependence of various device parameters, including the film structure, roughness, and interfacial properties. Further studies are needed in order to understand this effect.

V. CONCLUSIONS

The low-voltage transport in metal-organic sandwich devices with palladium and gold electrodes and CuPc and CoPc as organic layers is linear, i.e., Ohmic, for a wide range of temperatures and organic layer thicknesses. The conductance depends exponentially on temperature and thickness. The exponential decrease of the conductance with thickness becomes steeper at lower temperatures. For thicknesses larger than

100 nm, the conductance decreases at a much smaller rate. The exponential thickness dependence can not be explained with a coherent tunneling model because the devices have thicknesses of at least 210 Å.

The conventional models (nearest-neighbor or variable-range hopping), commonly used to describe the temperature behavior of the conductivity, suggest the existence of multiple transport regimes as a function of temperature. On the other hand, the conductance of all devices can be universally described with an exponential dependence across the whole temperature range. A similar exponential increase of the conductivity has been previously observed for a wide range of low-conductivity, inorganic semiconductors, and was fitted with a tunneling model based on the thermal variation of localized-states wave-function overlap.²⁶ Using the same concept, a generalized model is derived here, and the conductance of the devices is calculated. By assuming that molecular fluctuations produce tunneling paths between localized states with fluctuating barrier widths and heights, the exponential dependence of conductance on thickness and temperature was obtained. Interestingly, the temperature and thickness dependence allow the decoupling of the contributions to the conductance from the film and the electrode-film interface.

ACKNOWLEDGMENTS

C. N. Colesniuc acknowledges Professor M. Di Ventra for helpful discussions, and Dr. B. Fruhberger and Professor A. Sharoni for help with the sample fabrication and data acquisition. We thank Professor M. M. Fogler for critical reading of the manuscript and criticism of the ideas presented here. Work was supported by an AFOSR STTR contract and the DOE under Contract No. DE-AC52-06NA25396, the UCOP funds T027, and by the UCOP program on carbon nanostructures. S. A. Hevia also acknowledges support from the CONICYT foundation.

*ccoles@physics.ucsd.edu

¹C. C. Leznoff and A. B. P. Lever (Eds.), *Phthalocyanines: Properties and Applications* (Wiley-VCH, New York, 1989).

²G. Witte and C. Woll, *J. Mater. Res.* **19**, 1889 (2004).

³D. Parker, *J. Appl. Phys.* **75**, 1656 (1994).

⁴W. M. Blom, M. J. M. de Jong, and J. J. M. Vleggaar, *Appl. Phys. Lett.* **68**, 3308 (1996).

⁵K. R. Rajesh and C. S. Menon, *J. Non-Cryst. Solids* **351**, 2414 (2005).

⁶Q. Zhou and R. D. Gould, *Thin Solid Films* **317**, 432 (1998).

⁷A. Ahmad and R. A. Collins, *Thin Solid Films* **217**, 75 (1992).

⁸P. E. Burrows, Z. Shen, V. Bulovic, D. M. McCarty, S. R. Forrest, J. A. Cronin, and M. E. Thompson, *J. Appl. Phys.* **79**, 7991 (1996).

⁹A. Ioannidis, E. Forsythe, Y. Gao, M. W. Wu, and E. M. Conwell, *Appl. Phys. Lett.* **72**, 3038 (1998).

¹⁰P. W. M. Blom, C. Tanase, D. M. de Leeuw, and R. Coehoorn, *Appl. Phys. Lett.* **86**, 092105 (2005).

¹¹M. A. Baldo and S. R. Forrest, *Phys. Rev. B* **64**, 085201 (2001).

¹²B. N. Limketkai and M. A. Baldo, *Phys. Rev. B* **71**, 085207 (2005).

¹³M. Samuel, C. S. Menon, and N. V. Unnikrishnan, *J. Phys.: Condens. Mat.* **18**, 135 (2006).

¹⁴F. Schreiber, *Phys. Stat. Sol. A* **201**, 1037 (2004).

¹⁵H. Peisert, T. Schwieger, J. M. Auerhammer, M. Knupfer, M. S. Golden, J. Fink, P. R. Bressler, and M. Mast, *J. Appl. Phys.* **90**, 466 (2001).

¹⁶H. Haick, J. Ghabboun, and D. Cahen, *Appl. Phys. Lett.* **86**, 042113 (2005).

¹⁷R. Schmechel, *J. Appl. Phys.* **93**, 4653 (2003).

¹⁸V. Ambegaokar, B. I. Halperin, and J. S. Langer, *Phys. Rev. B* **4**, 2612 (1971).

¹⁹R. E. Holmlin, R. Haag, M. L. Chabinyk, R. F. Ismagilov, A. E. Cohen, A. Terfort, M. A. Rampi, and G. M. Whitesides, *J. Am. Chem. Soc.* **123**, 5075 (2001).

²⁰D. J. Vold, R. Haag, M. A. Rampi, and C. D. Frisbie, *J. Phys. Chem. B* **106**, 2813 (2002).

²¹M. P. Samanta, W. Tian, S. Datta, J. I. Henderson, and C. P. Kubiak, *Phys. Rev. B* **53**, R7626 (1996).

- ²²H. Steinberg, Y. Lilach, A. Salant, O. Wolf, A. Faust, O. Millo, and U. Banin, *Nano Lett.* **9**, 3671 (2009).
- ²³A. J. Campbell, D. D. C. Bradley, and D. G. Lidzey, *J. Appl. Phys.* **82**, 6326 (1997).
- ²⁴D. R. Stewart, D. A. A. Ohlberg, P. A. Beck, C. N. Lau, and R. S. Williams, *Appl. Phys. A* **80**, 1379 (2005).
- ²⁵F. A. Padovani and R. Stratton, *Solid State Electron* **9**, 695 (1966).
- ²⁶C. M. Hurd, *J. Phys. C: Solid State Phys.* **18**, 6487 (1985).
- ²⁷N. Marom, O. Hod, G. E. Scuseria, and L. Kronik, *J. Chem. Phys.* **128**, 164107 (2008).